ISSN: 2634-9221
European Journal of Applied Sciences; Vol. 14 No. 02 (2026) (14-30)
https://doi.org/10.14738/aivp.1402.20043

Biodiesel Production from Waste Cooking Oil using Modified Poultry Droppings as Catalyst. Response Surface Methodology, Artificial Neural Network, and Extreme Gradient Boosting as Modeling and Optimization Tools

David Ohimai Ahonkhai, Kessington Obahiagbon, & Eghe Amenze Oyedoh

1. Department of Chemical Engineering, University of Benin, Nigeria

Abstract: Poultry droppings catalyst was modified with nickel sulphate for the synthesis of biodiesel from waste cooking oil (WCO) with 6.43 % free fatty acid. The catalyst modified was characterized using Brunauer Emmet Teller (BET), Fourier Transform Infrared Spectroscopy (FTIR), Scanning Electron Microscopy and Energy dispersive X-ray (SEM-EDX), X-ray diffraction (XRD), and X-ray fluorescent analysis (XRF). Response surface methodology (RSM), artificial neural network (ANN), and extreme gradient boosting (XGB) were employed in modeling and optimizing the process conditions. Box-Behken design (BBD) of four process variables was used in designing the experiment. The biodiesel produced was characterized and its properties compared with established standards. The reusability potential of the catalyst was also assessed. The catalyst characterization revealed high surface area of 355.36 m^2/g. Acidic and basic oxides such as CaO, SiO_2, NiO, SO_3, Al_2O_3 and Fe_2O_3 in significant quantities were found present indicating its bi-functionality. Optimum biodiesel yield of 96.82 % was obtained with methanol/oil ratio of 12.98:1, catalyst loading of 3.66 wt.%, temperature of 59℃, and reaction time of 86.45 minutes. RSM, ANN and XGB model were found to be efficient in modeling biodiesel production process with XGB performing best with the highest R^2 value of 0.9915. The properties of biodiesel produced were within the acceptable limits when compared with ASTM D6751 and EN 14214 standards.

Keywords: RSM, ANN, XGB, Poultry droppings, Modeling,

INTRODUCTION

Over the past decades, human activity has increased dramatically. As time goes on, the need for energy as electricity, transportation fuels, heating fuels, and industrial processes has increased also. This rise in demand and consumption can be linked to the world's population growth and rapid economic development. Furthermore, energy resources are regarded as the foundation and most important tool for any nation's socioeconomic development [1]. Conventional sources of energy which are not renewable has been depleted due to uncontrolled extraction and excessive consumption caused by the aforementioned issue.

This has prompted the search for an alternative fuel that supports energy conservation, sustainable development, effective management, and environmental preservation in the modern world [2]. Biofuels have been found to be the best option when taking economic expenses and environmental considerations into account. Biodiesel made from oils is being researched as a potential substitute for conventional fuels among the

various forms of biofuels, which are becoming more and more recognized as viable alternatives to fossil fuels [3].

Transesterification of triglycerides with alcohol using an appropriate catalyst produces biodiesel [4]. Edible oils are used as a feedstock in the majority of conventional biodiesel manufacturing processes, which are typically catalyzed by homogeneous catalysts [5]. Utilizing non-edible oil feedstock like waste cooking oil (WCO) to produce biodiesel is crucial because it lowers the assets and liabilities associated with using edible oils, while minimizing WCO disposal [6]. According to Khan et al. [7], biodiesel has several advantages, such as being biodegradable, renewable, less hazardous, having a higher cetane number, and having a higher flash point. The manufacture of biodiesel improves environmental conditions by lowering fuel prices, raising productivity, and lowering pollution levels in the land, water, and atmosphere.

Process variables such as methanol/oil ratio, catalyst loading, reaction time, reaction temperature, and agitation speed, are amongst the process parameters that affect biodiesel production process. Optimizing these process variables can ensure optimal performance of the biodiesel production process. Conventional optimization techniques often fail to capture nonlinear or interacting effects among variables. In this study, Response surface methodology (RSM), artificial neural network (ANN) and extreme gradient boosting (XGB) were used as tools for modeling and optimization. RSM is a statistical method that may be used to predict, optimize, and plan trials with numerous process variables, resulting in acceptable results with fewer experiments and lower costs [8]. ANN is a group of mathematical methods for machine learning, regression, and statistical analysis of frequently complex data that are inspired by biology (a simplified model of the human brain) [9]. Large datasets and significant processing power are needed for ANNs, which reduce interpretability and add a level of individual uncertainty due to input variance [10]. By effectively handling noisy data and generating precise predictions with its gradient-boosting technique, XGB enhances these methods [11]. Because to its regularization methods, speed, and scalability, XGB is frequently used [12]. When combined, these models offer insights into the ways that various input variables affect the process of producing biodiesel.

MATERIALS AND METHODS

Materials

WCO was collected from a local restaurant within Benin City, Nigeria. The collected WCO was first filtered with to remove traces of food particles and then heated at 100^{o}C to lower the content of moisture. Poultry droppings for catalyst preparation was obtained from a poultry in Benin City, Nigeria. Nickel sulphate and other analytical grade reagents used were purchased from a vendor.

Catalyst Preparation

Poultry droppings obtained was sun-dried for several days to remove moisture and then grinded to reduce the particle size. The powdered dry poultry droppings was then heated to 300°C in a carbonization process for 3 hours in a muffle furnace. The sample was then treated with 0.1M KOH, and calcined for 4 hours in a muffle furnace at 900°C [13]. Using

sol-gel method, nickel sulphate was dissolved in a mixture of hydrochloric acid and distilled water, then it was combined with the calcined poultry dropping. The mixture was stirred for 1 hour to ensure homogeneity. Deionized water and ammonia solution were added slowly to adjust the pH to 9, promoting gel formation, and it was stirred at 60°C for 2 hours. The resulting gel was kept for 24 hours at room temperature to enhance the structural integrity of the gel and then dried afterwards at 100°C for 12 hours using an oven [14]. The dried gel was then calcined at 500°C for 4 hours in a muffle furnace.

Catalyst Characterization

Different analyses was conducted on the catalyst to determine its surface area, pore volume and diameter, morphology, structure and the different composition of the catalyst. The analyses included BET analysis FTIR spectroscopy analysis, SEM-EDX analysis, XRD analysis and XRF analysis.

Biodiesel Production and Characterization

Biodiesel was produced by a method described by Obahiagbon et al., [4]. As specified by the experimental design, a specific amount of WCO was measured into a conical flask, then heated on the magnetic stirrer to a specific temperature. The catalyst was measured into a beaker and measured methanol was added. The methanol and catalyst were mixed and the resulting solution emptied into the heating oil. The reaction time was then set as stipulated by the design. The mixture was allowed to react until reaction time was completed. The mixture was then separated using a centrifuge and after which, washed with warm distilled water to remove any trace of methanol, glycerol and unreacted triglycerides, diglycerides, monoglycerides and acids that may be contained in it. The washing process was continued until the washed water appeared clear. The washed biodiesel was thereafter dried [15]. Biodiesel yield was calculated using Equation (1).

$$\text{Biodiesel yield} = \frac{\text{mass of biodiesel produced}}{\text{mass of WCO used}} \times 100 \quad (1)$$

Experimental Design and RSM Modelling

The experiment with four input process variable variables (methanol/oil ratio, catalyst loading, reaction temperature and reaction time) was designed using Box Behken Design (BBD) with response being biodiesel yield. The BBD resulted in 29 experimental runs, which was randomly performed in the Laboratory to avoid any systematic error in the outcomes. Table 1 shows the coded and actual levels of the BBD variables. The experimental data were analyzed by response surface regression using the second order polynomial shown in Equation (2) [13].

$$Y_i = b_o + \sum b_i X_i + \sum b_{ij} X_i X_j + \sum b_{ii} X_i^2 + e_i \quad (2)$$

Where,

Y_i denotes the predicted response,

b_o is the value at intercept,

b_i is the coefficient of first order,

b_{ii} is the quadratic effect coefficient,

b_{ij} is the interacting effect coefficient,

X_i and X_j are the process variables that affect the response, and

e_i is the experimental random error.

Table 1: Coded and actual levels of BBD variables

Process variables	Units	Factor	Coded Low	Mean	Coded High
Methanol/oil ratio	-	A	6	12	18
Catalyst loading	Wt.%	B	1	3	5
Reaction temperature	°C	C	40	55	70
Reaction time	Min.	D	60	90	120

ANN Modeling

ANN was used to model the biodiesel production process. This was accomplished using Matrix Laboratory (MATLAB) version R2021a. A feed forward ANN with three layers: an input layer (four neurons for methanol/oil ratio, catalyst loading, reaction temperature, and reaction time), one hidden layer and an output layer (one neuron for the response). The experimental data were split into training (60%), validation (25%), and testing (15%) datasets. The backpropagation algorithm was used for training with the mean squared error (MSE) as the performance metric. The trained ANN model was validated using the testing dataset, and its predictive capability was evaluated by comparing the predicted responses with the experimental results. The trained ANN was also used to simulate different combinations of machining parameters, and the optimal parameters were selected based on the desired responses [16].

XGB Modeling

To develop the XGB machine learning model for predicting biodiesel yield, Python was used. The study adopted the grid search technique to configure the model parameters. Input parameters such as methanol/oil ratio, catalyst loading, reaction temperature, and reaction time were incorporated into the model. 80% of the data was dedicated to training the algorithm, while the remaining 20% was utilized for the testing phase. In supervised machine learning, overfitting is a common challenge that can lead to inaccurate predictions on new data.

To mitigate this risk, cross-validation was employed. In this method, the test dataset remained untouched and was reserved solely for the final evaluation. Subsets for training and validation were created from the training dataset for model assessment. Through multiple iterations, the model outputs were averaged to generate the final predictions. The k-fold cross-validation technique was employed in the proposed approach, where training and testing were carried out for each fold [17].

Comparative Performance of RSM, ANN and XGB

Statistical parameters were used to assess the performance of the RSM, ANN and XGB models in predicting the biodiesel yield. These include goodness-of-fit metrics and error terms such as coefficient of determination (R^2), mean square error (MSE), and root mean square error (RMSE), as presented in Equations (3) – (5). Good predictive performance is indicated by high R2 value usually close to unity with low MSE and RMSE values [18].

$$R^2 = 1 - \frac{\sum_{i=1}^{n}(x_{a,i} - x_{p,i})^2}{\sum_{i=1}^{n}(x_{p,i} - x_{a,ave})^2} \quad (3)$$

$$MSE = \frac{1}{n}\sum_{i=1}^{n}(x_{p,i} - x_{a,i})^2 \quad (4)$$

$$RMSE = \sqrt{\frac{1}{n}\sum_{i=1}^{n}(x_{p,i} - x_{a,i})^2} \quad (5)$$

Where,

n is the number of experimental runs,

$X_{p,i}$ is the estimated values,

$X_{a,i}$ is the experimental values,

$X_{a,ave}$ is the average experimental values.

RESULTS AND DISCUSSIONS

Properties of the WCO

The properties of the WCO used in this study are presented in Table 2. The results obtained from the analysis corresponded with analysis of WCO by previous studies [19, 20].

Table 2: Physicochemical properties of WCO

Properties	Value
Acid value (mg KOH/g)	13.86
FFA (%)	6.43
Saponification value (mg KOH/g)	205.97
Iodine value (g/100g)	102.5
Peroxide value (meq/Kg)	8.6
Density (kg/cm^3)	920
Viscosity (mm^2/s @40^{o}C)	36
Molecular weight	876.06

Catalyst Characterization

BET Analysis

The BET analysis revealed that the catalyst had a large surface area of 355.36 m^2/g, pore volume of 0.23 cc/g, and pore diameter of 2.41 nm. High surface area, pore volume and diameter will facilitate faster diffusion of reactants and products from the pores to the

reaction sites to the catalyst surface. It also indicates increased reusability of the catalyst, which is highly desired. These characteristics confirms that the modified catalyst is suitable for biodiesel production.

FTIR Analysis

The FTIR data of the catalyst is shown in Figure 1, elucidating the catalyst's functional group composition. Peaks occurred at 3229.7 cm^{-1}, 2161.9 cm^{-1}, 1638.2 cm^{-1}, 1094.0 cm^{-1}, 984.0 cm^{-1}, 900.2 cm^{-1}, 721.2 cm^{-1}, and 676.5 cm^{-1}. The large peak seen at 3229.7 cm^{-1} suggests the presence of hydroxyl linked to the O-H stretch functional group. The presence of a C ≡ C stretch is indicated by the peak at 2161.9 cm^{-1}. The presence of C-H stretch was shown by peak at 1638.2 cm^{-1}. 1094.0 cm^{-1}, 984.0 cm^{-1}, and 676.5 cm^{-1} indicates the presence of aromatic rings due to C-H bends. 900.2 cm^{-1} and 721.2 cm^{-1} demonstrates the C-C vibrations indicating the presence of alkane/alkyl groups. Catalysts developed from poultry droppings characterized by similar peaks have been reported by Maneerung et al., [21] and Alaneme et al., [22].

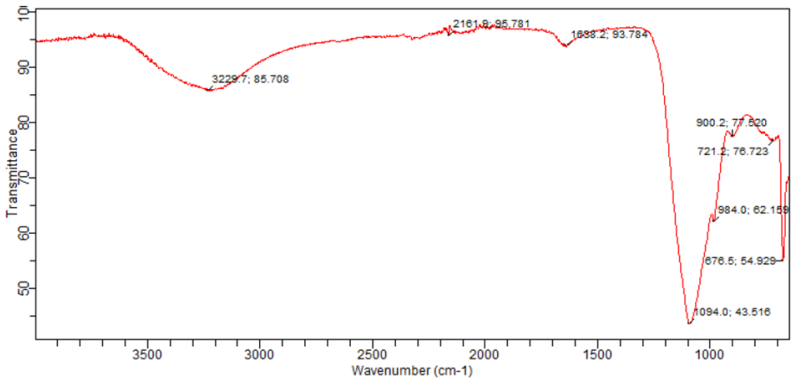

Figure 1: FTIR spectra of catalyst

SEM-EDX Analysis

The morphological structure of the catalyst was characterized via SEM as shown in Figure 2. A rough irregular flake-like structure can be observed, with the presence of high porosity which is desired as attachment sites for reaction to occur. The pores were seen to be distributed throughout the catalyst with the presence of smaller particles agglomerations. The morphology of the catalyst observed can be caused by the nature of the catalyst precursor, which vary in composition and surface properties. Presence of high surface area enhances the catalytic activities of heterogeneous catalysts [15]

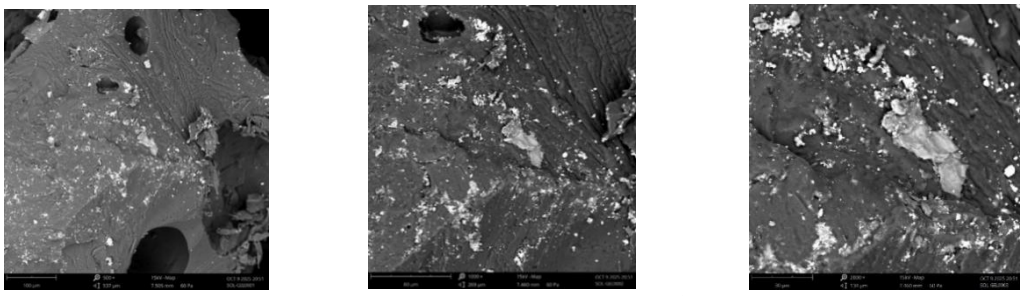

Figure 2: SEM images of catalyst

The EDX pattern showed on Figure 3 indicates that the catalyst had within it elements like calcium, sulphur, zinc iron, and silicon. The elements present in the catalyst are very reactive, explaining the catalytic behavior of the catalysts and also indicating the incorporation of nickel sulfate through the sol-gel modification method.

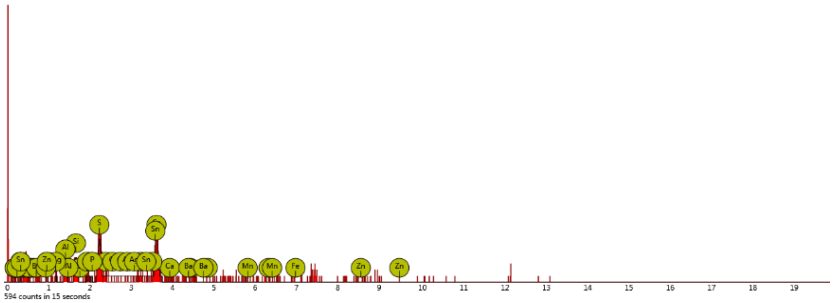

Figure 3: EDX pattern of the catalyst

XRD Analysis

The XRD data of the catalyst is shown in Figure 4. This analysis revealed a sharp crystallinity spectrum at 2θ values of 21.06°, 25.63°, 26.76°, 31.49°, 36.49°, 42.47° and 43.50° attributed to the presence of sanidine ($K(AlSi_3O_8)$), quartz (SiO_2), barite (Ba(SO)), gypsum ($Ca(SO_4)(H_2O)_2$), and nickelboussingaultite ($(NH_4)_2Ni(SO_4)$-$6H_2O$). The high crystallinity of the material shows a high degree of structural orientation in the catalyst with major peaks indicating the presence of CaO and SiO_2 contributing to the reactivity of the catalyst. Similar peaks and crystalline structures have been reported for catalysts with CaO presence by previous studies [22, 24].

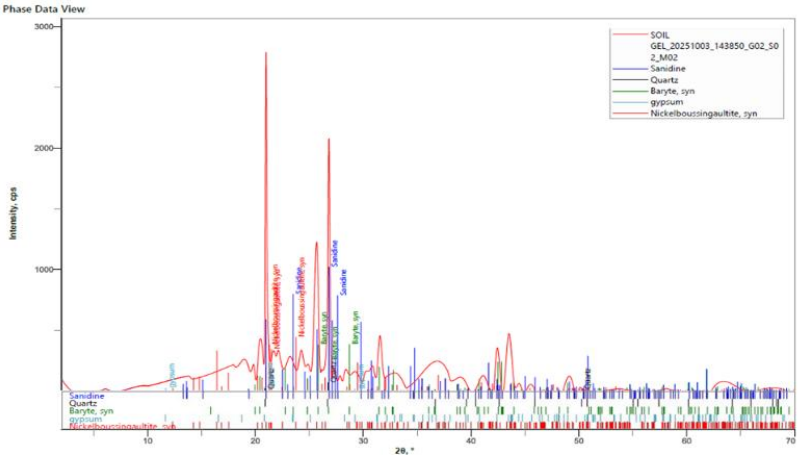

Figure 4: XRD result for the catalyst

XRF Analysis

The XRF data of the catalyst is presented in Table 3. CaO of 26.926 % constitutes the largest proportion of the catalyst's composition. CaO is highly desirable for biodiesel production because of its low toxicity and its ability to enhance transesterification [25]. Other metallic oxides found in significant present were SiO_2, NiO, SO_3, Al_2O_3 and Fe_2O_3. The significant presence of NiO in the catalyst composition confirms the successful modification of the

poultry droppings. These oxides found have been reported to be active materials for biodiesel production by Husin et al., [26] and Mahmood et al., [27]

Table 3: XRF data for catalyst

Component	Concentration (%)
Silicon oxide (SiO_2)	16.761
Iron (iii) oxide (Fe_2O_3)	5.552
Nickel oxide (NiO)	20.245
Trioxosulphate (SO_3)	10.720
Calcium oxide (CaO)	26.926
Magnesium oxide (MgO)	3.903
Aluminum oxide (Al_2O_3)	9.430

Process Modeling and Optimization

RSM Modeling

Experimental yield from the biodiesel production process and the predicted yield with the experimental conditions as generated from the BBD are shown in Table 4. The predicted responses for the biodiesel production process were calculated using a second-degree polynomial given by Equation (6). It presents the quadratic model equation developed using RSM in terms of the coded values.

$$\dot{Y} = -406.58 + 17.09A + 16.11B + 7.49C + 3.09D + 0.93AB - 0.05AC - 0.04AD + 0.57BC - 0.23BD + 0.02CD - 0.51A^2 - 5.68B^2 - 0.09C^2 - 0.02D^2 \quad (6)$$

Table 5 shows the ANOVA results, which indicated that the quadratic mathematical model obtained in this study is significant at p-value < 0.05. The F-value of 0.7333 and the p-value of 0.6864 implies the lack of fit is not significant relative which is desirable. The fit statistics data showed R^2 of 0.9897, adjusted R^2 of 0.9795 and predicted R^2 of 0.9561. High R^2 value shows good agreement between the RSM predicted and experimental values.

Table 4: Experimental design with Experimental, RSM, ANN and XGB response

Run	A	B	C	D	Responses			
	-	Wt%	°C	Mins	EXP	RSM	ANN	XGB
1	18	1	55	90	37.61	39.61	38.32	37.95
2	6	3	55	60	46.83	47.08	46.98	47.10
3	12	3	55	90	95.67	94.27	92.65	95.07
4	12	3	40	120	45.72	48.47	45.61	46.27
5	12	1	70	90	34.28	35.47	34.39	35.66
6	6	3	70	90	62.04	64.68	61.22	62.07
7	18	3	55	60	72.51	71.19	72.25	72.28
8	12	3	70	120	81.09	79.46	80.45	80.03
9	12	3	55	90	95.67	94.27	92.65	95.07
10	12	3	55	90	88.65	94.27	92.65	95.07

11	12	3	55	90	95.67	94.27	92.65	95.07
12	18	5	55	90	74.63	76.32	75.04	73.74
13	6	3	55	120	67.51	67.78	64.07	67.10
14	12	5	70	90	85.87	83.96	86.92	85.61
15	12	5	55	120	52.23	53.89	57.42	53.04
16	6	5	55	90	45.46	44.43	44.29	46.52
17	6	3	40	90	40.11	38.71	40.15	46.27
18	18	3	70	90	62.05	63.54	62.19	62.08
19	12	5	40	90	36.61	34.37	37.89	38.68
20	12	1	55	120	69.42	67.68	69.04	68.87
21	12	1	40	90	53.45	54.3	54.38	53.63
22	18	3	55	120	63.89	62.58	63.33	63.83
23	6	1	55	90	53.31	52.59	54.35	50.66
24	18	3	40	90	61.31	58.76	61.63	61.39
25	12	1	55	60	35.13	33.56	34.69	35.66
26	12	3	55	90	95.67	94.27	92.65	95.07
27	12	3	40	60	55.44	58.04	55.36	55.57
28	12	3	70	60	59.59	57.81	60.66	60.48
29	12	5	55	60	74.08	75.91	74.84	73.89

Table 5: ANOVA analysis for quadratic model

Source	Sum of Squares	df	Mean Square	F-value	p-value	
Model	10778.27	14	769.88	96.50	< 0.0001	Significant
A-Methanol/oil	268.29	1	268.29	33.63	< 0.0001	
B-Catalyst Loading	611.76	1	611.76	76.68	< 0.0001	
C-Reaction Temperature	709.63	1	709.63	88.95	< 0.0001	
D-Reaction Time	109.69	1	109.69	13.75	0.0023	
AB	503.33	1	503.33	63.09	< 0.0001	
AC	112.25	1	112.25	14.07	0.0021	
AD	214.62	1	214.62	26.90	0.0001	
BC	1170.67	1	1170.67	146.73	< 0.0001	
BD	787.92	1	787.92	98.76	< 0.0001	
CD	243.67	1	243.67	30.54	< 0.0001	
A^2	2176.04	1	2176.04	272.75	< 0.0001	
B^2	3346.37	1	3346.37	419.44	< 0.0001	
C^2	2473.68	1	2473.68	310.05	< 0.0001	
D^2	1234.11	1	1234.11	154.68	< 0.0001	
Residual	111.70	14	7.98			
Lack of Fit	72.27	10	7.23	0.7333	0.6864	not significant
Pure Error	39.42	4	9.86			
Cor Total	10889.97	28				

The effects of input process parameters on biodiesel production yield were analyzed by three- dimensional (3D) surface plots. Figure 4 shows the 3D surface plots representing two independent variables while keeping other variables constant. An increase in methanol /oil ratio, there was an increase in the biodiesel yield with maximum yield obtained at 12:1, also a gradual reduction in biodiesel yield was observed beyond 12:1 methanol/oil ratio. Previous studies have shown that excess methanol results in low biodiesel yield as a result of an increase in the polarity of the reaction mixture which increases the solubility of glycerol and therefore favours the reverse reaction during biodiesel production process [7, 28]. The effect of catalyst loading, investigated within the range of 1 to 5 wt% , 3 wt% was sufficient to obtain the maximum biodiesel yield. Increasing the catalyst loading further resulted in a gradual reduction in the biodiesel yield. Gouran et al., [29] reported similar observation using wheat bran ash to produce biodiesel from waste cooking oil. Increase in reaction temperature, resulted an increase in the biodiesel yield with maximum yield obtained at 55ºC, also a gradual reduction in biodiesel yield was observed beyond 55ºC. Previous studies have reported an increase in biodiesel yield with an increase in reaction temperature is consistent with the provisions of Arrhenius equation, which indicates increase in rate of reaction with increase in temperature [30]. Increase in reaction time, there was an increase in the biodiesel yield with maximum yield obtained after 90 minutes. A gradual reduction in biodiesel yield was observed increasing the duration above 90 minutes. Some previous reports showed that with increase in time during biodiesel production process, there is an increased biodiesel yield [31].

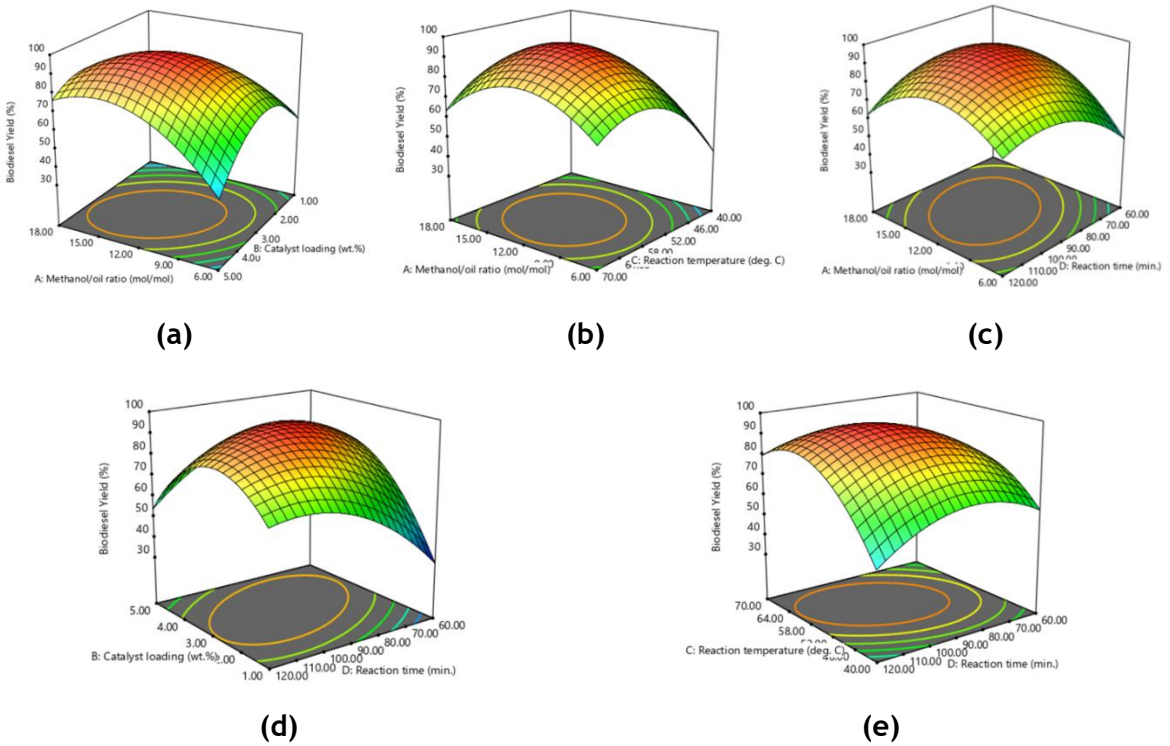

Figure 4: 3D plots showing the interaction between (a) Methanol/oil ratio and catalyst loading (b) Catalyst loading and reaction temperature and (c) methanol/oil ratio and reaction time (d) catalyst loading and reaction time (e) reaction temperature and reaction time

ANN Modeling

An optimum neural network architecture shown in Figure 5 was generated and employed to predict the yield from biodiesel production. Figure 6 showing the regression plot reveals the correlation coefficient between the actual target values from biodiesel production process yield and the predictions made by the trained neural network on the training dataset (R=0.7624), the validation dataset (R=0.95153), the test dataset (R=0.99657) and the overall dataset (R=0.82714) which suggests that the neural network's predictions are positively correlated with the actual target values. These values obtained indicates a relatively strong positive correlation between the predicted and actual values for all catalyzed processes and signifies robust prediction for the yields of the various biodiesel production processes. Upon completion of the network training and testing, the predicted values for the yields using the different catalyst are shown in Table 4.

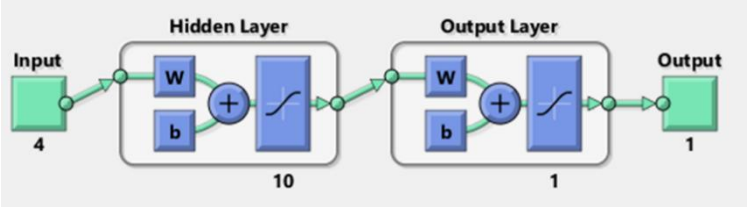

Figure 5: ANN model architecture

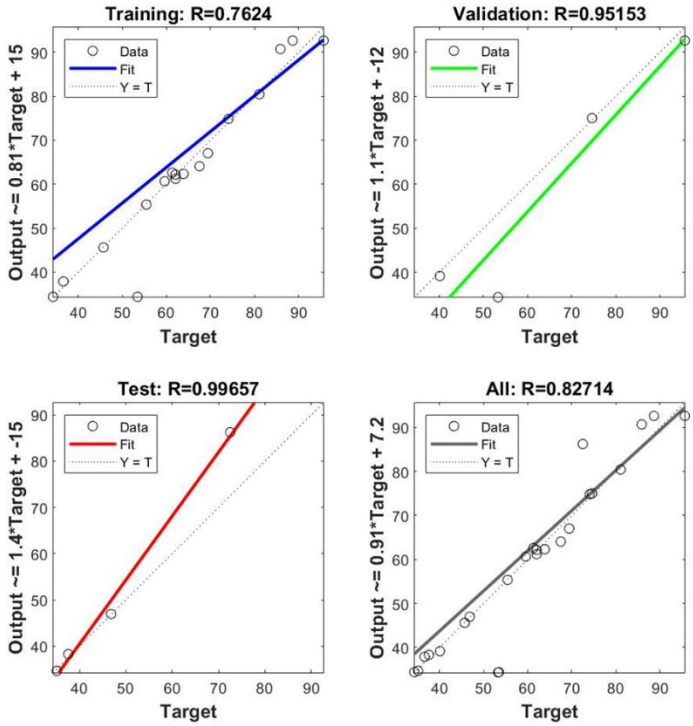

Figure 6: Regression plot of training, validation and testing

XGB Modeling

RSM and ANN were effective in predicting the optimal values of the input needed to maximize yield using the various catalyst produced. Although, the ensemble size and depth of XGB enhance robust gradient boosting for predicting biodiesel yield. Collectively, these

optimized configurations serve to contribute to the high predictive performance of the models. The optimized hyperparameters (n_estimators, learning_rate, max_depth, subsample, and colsample_bytree) were incorporated into each machine learning model to predict biodiesel yield as a function of the inputs. SHapley Additive ExPlanation (SHAP) analysis was carried out to unravel the influence of methanol/oil ratio, catalyst loading, reaction temperature, and reaction time on biodiesel yield predictions. The SHAP beeswarm plot in Figure 7 shows the local explanations of the contributions of each feature to the model's output. The plot shows the extent of each feature's influence on biodiesel yield prediction, with the horizontal axis denoting SHAP values and the vertical axis ranking input features by significance. Each point represents a sample, color-coded by the feature's actual value.

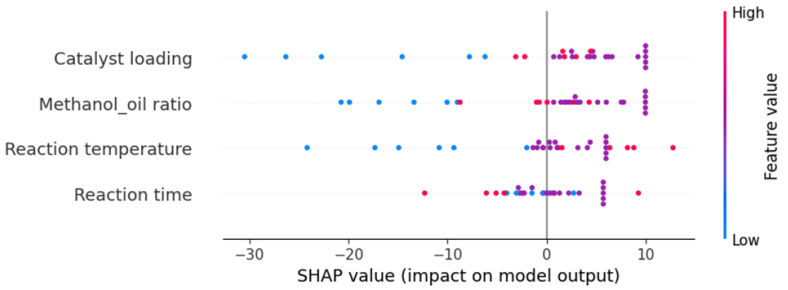

Figure 7: Beeswarm plot showing feature importance for the input variables

Catalyst loading (-30 to +10) demonstrated the most extensive SHAP range, affirming its status as the most significant variable. This suggests that optimizing catalyst loading could relatively improve efficiency of the process. Methanol/oil ratio (-20 to +10) exhibited a narrow and consistent contribution, indicating that methanol/oil ratio can be optimized to increase yield without impactful fluctuations. Reaction temperature (-25 to +12) exhibited a narrower and more consistent contribution, indicating that catalyst weight can be optimized to maintain yield. Reaction time showed the least SHAP variation (-12 to +10), suggesting that higher time duration modestly improved biodiesel yield.

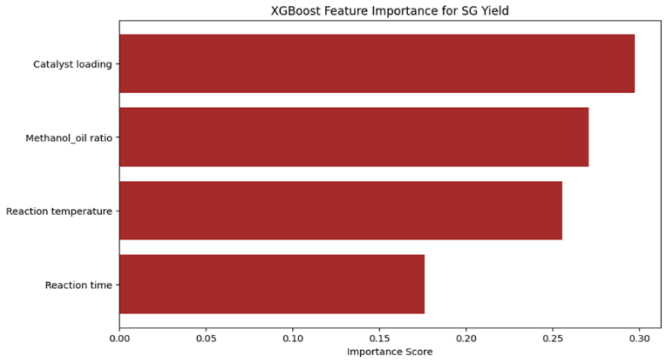

Figure 8: Global SHAP feature-importance ranking plot for the input features

These findings are consistent with the global SHAP ranking and the SHAP waterfall plot in Figure 8 and 9 respectively, where catalyst loading is predominant, followed by methanol/oil ratio, reaction temperature and reaction time. From the SHAP waterfall plot,

catalyst loading, methanol/oil ratio, reaction temperature and reaction time contributed +9.96, +9.94, +5.97 and +5.69 respectively to the process.

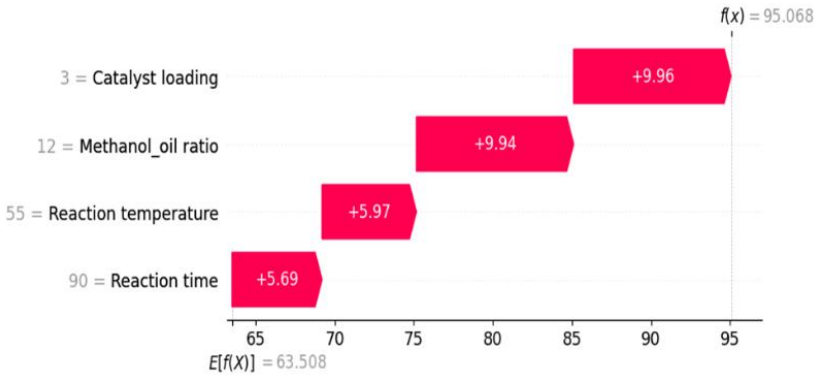

Figure 9: SHAP waterfall plot for the optimized inputs

Comparison of Performance of the RSM, ANN and XGB Models

The goodness of fit metrics for RSM, ANN and XGB models, were evaluated and presented in Table 6. RSM, ANN and XGB demonstrated strong predictive capacity, as seen in their high R^2 values of 0.9897, 0.9914, and 0.9915 respectively. R^2 value is a key measure of model fit, indicating how well the variability in the output was explained by the input. To evaluate further the prediction reliability, error-based performance metrics such as MSE and RMSE were employed. These quantified the difference between experimental data and model predictions, with lower values indicating better predictive performance. XGB model outperformed the RSM and ANN models with a higher R^2 and lower MSE and RMSE values.

Table 6: Comparison of RSM and ANN performance

Statistical parameters	RSM	ANN	XGB
R^2	0.9897	0.9914	0.9915
MSE	3.8502	3.506	3.442
RMSE	1.9622	1.8725	1.8553

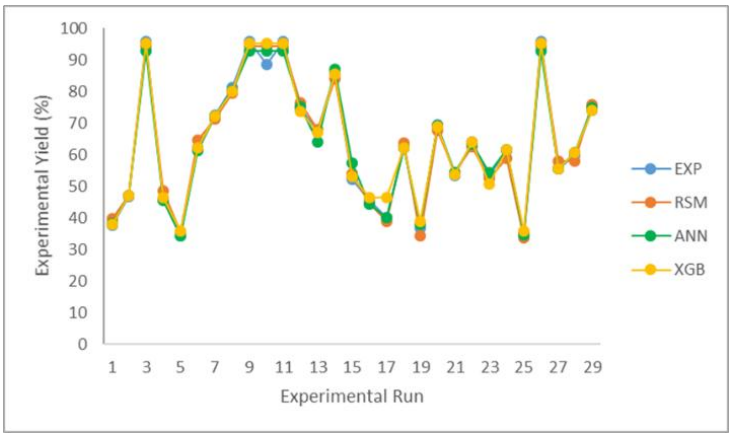

Figure 10: Time series plot of Experimental, RSM, ANN and XGB data for biodiesel yield

Figure 10 shows that RSM, ANN and XGB predictions are in good agreement with the experimental value, but XGB predicted value shows a better correlation with the experimental values obtained. This visualization complements the statistical indicators provided in Table 6, indicating the models' effective performance. The superiority of XGB model has been confirmed by previous studies [17, 32]

Numerical Optimization of Biodiesel Yield

In this study, numerical optimization was used for the optimization of the biodiesel production process. The optimal conditions chosen was that which gave the maximum biodiesel of 96.86 % achieved with a methanol/oil ratio of 12.98:1, catalyst loading of 3.66 wt.%, temperature of 59℃, and reaction time of 86.45 minutes.

Biodiesel Characterization

The physicochemical properties of the biodiesel produced at optimum conditions were analyzed and the results are presented in Table 7. The properties of the biodiesel are well within the required standard as compared to ASTM D6751and EN14214 standards of biodiesel. Fatty acid profile of the biodiesel produced is presented in Table 8.

Table 7: Physicochemical properties of biodiesel produced and standards of biodiesel

Properties (units)	Biodiesel produced	ASTM D6751	EN14214
Acid value (mg KOH/g)	0.43	0.8max	0.5max
Flash point (°C)	149	>130	>120
Calorific value (MJ/kg)	40.59	35	-
Cetane number	55.18	>47	>51
Viscosity at 40°C (mm^2/s)	5.15	1.9 – 6	3.5 – 5
Density (kg/m^3)	894	-	860-900

Table 8: Fatty acid profile of produced biodiesel

Fatty acid	Nature	Chemical formula	Retention time (min)	Area (%)
Palmitic acid	Saturated	$C_{16}H_{32}O_2$	13.901	11.64
Myristic acid	Saturated	$C_{15}H_{30}O_2$	11.743	1.76
Stearic acid	Saturated	$C_{18}H_{36}O_2$	17.180	3.97
Linoleic acid	Unsaturated	$C_{18}H_{32}O_2$	16.419	52.78
Gondoic acid	Unsaturated	$C_{20}H_{38}O_2$	20.343	1.55
Oleic acid	Unsaturated	$C_{18}H_{34}O_2$	37.161	15.10
Erucic acid	Unsaturated	$C_{22}H_{42}O_2$	23.426	11.35
Others				1.75

CONCLUSION

Catalyst was created from poultry droppings modified with nickel sulphate using sol-gel method. The catalyst contained both acidic and basic oxides and it was successfully used

for the transesterification of WCO. RSM, ANN and XGB were effective in biodiesel yield predictions with high R^2 values of 0.9897, 0.9914, and 0.9915 respectively. XGB model performed best having the highest R^2 value and lowest MSE and RMSE values. Optimum biodiesel yield of 96.86 % was achieved with a methanol/oil ratio of 12.98:1, catalyst loading of 3.66 wt.%, temperature of 59℃, and reaction time of 86.45 minutes. The physicochemical properties of the biodiesel produced at these conditions were within the ASTM D6751 and EN 14214 standards.

ACKNOWLEDGEMENT

This study was supported by the Petroleum Technology Development Fund (PTDF), through the PTDF Professorial Chair on Renewable Energy in the Department of Chemical Engineering, University of Benin, Nigeria.

REFERENCES

[1]. Nisar, J., Razaq, R., Farooq, M., Iqbal, M., Khan, R. A., Sayed, M., Shah, A., & Rahman, I., Enhanced biodiesel production from Jatropha oil using calcined waste animal bones as catalyst. Renewable Energy, 2017. 101, 111–119. https://doi.org/10.1016/j.renene.2016.08.048

[2]. Rouhany, M., and Montgomery, H., Global Biodiesel Production: The State of the Art and Impact on Climate Change. Springer International Publishing, 2019. https://doi.org/10.1007/978-3-030-00985-4_1

[3]. Ray, S. K., and Prakash, O., Biodiesel Extracted from Waste Vegetable Oil as an Alternative Fuel for Diesel Engine: Performance Evaluation of Kirlosker 5 kW Engine. Renewable Energy and Its Innovative Technologies, 2019. 219–229.

[4]. Obahiagbon, K., Nwafor, C., and Ahonkhai, D. O., Optimization of biodiesel production from rubber seed oil using a bifunctional catalyst derived from carbide slag and pig bones. Petroleum Technology Development Journal, 2024. 14(2), 16-30

[5]. Aniya, V. K., Muktham, R. K., Alka, K., and Satyavathi, B., Modeling and simulation of batch kinetics of non-edible karanja oil for biodiesel production: A mass transfer study. Fuel, 2015. 161, 137–145. https://doi.org/10.1016/j.fuel.2015.08.042

[6]. Ehsan, M., and Chowdhury, M. T. H., Production of biodiesel using alkaline based catalysts from waste cooking oil: A case study. Procedia Engineering, 2015. 105, 638–645. https://doi.org/10.1016/j.proeng.2015.05.042

[7]. Khan, H. M., Iqbal, T., Yasin, S., Ali, C. H., Abbas, M. M., Jamil, M. A., Hussain, A., Soudagar, M. E. M., and Rahman, M. M., Application of agricultural waste as heterogeneous catalysts for biodiesel production. Catalysts, 2021. 11(10), 1–17. https://doi.org/10.3390/catal11101215

[8]. Obahiagbon, K., and Ahonkhai, D. O., Optimized Biodiesel Production from Waste Cooking Oil Using Poultry Droppings Catalyst: A Comparison of RSM and ANN. Petroleum Technology Development Journal, 2023. 13 (2), pp. 1-19

[9]. Okpalaeke K. E., Ibrahim T. H., Latinwo L. M. and Betiku E., Mathematical Modeling and Optimization Studies by Artificial Neural Network, Genetic Algorithm and Response Surface Methodology: A Case of Ferric Sulfate–Catalyzed Esterification of Neem (Azadirachta indica) Seed Oil. Frontiers in Energy Research, 2020. 8 (614621), pp 1-14. DOI: 10.3389/fenrg.2020.614621

[10]. A.N. Amenaghawon, M.O. Omede, G.O. Ogbebor, S.A. Eshiemogie, S. Igemhokhai, N.I. Evbarunegbe, J.E. Ayere, B.E. Osahon, P.K. Oyefolu, S. O. Eshiemogie, C.L. Anyalewechi, M.O. Okedi, B.A. Chinemerem, H.S. Kusuma, H. Darmokoesoemo, I.G. Okoduwa, Optimized biodiesel synthesis from an optimally formulated ternary feedstock blend via machine learning-informed methanolysis using a composite biobased catalyst. Bioresour. Technol., 2024. 101805. https://doi.org/10.1016/J.BITEB.2024.101805.

[11]. O. Bongomin, C. Nzila, J.I. Mwasiagi, O. Maube, Exploring insights in biomass and waste gasification via ensemble machine learning models and interpretability techniques. Int. J. Energy, 2024. 6087208. https://doi.org/10.1155/ 2024/6087208.

[12]. T. Ali, S.U. Rehman, S. Ali, K. Mahmood, S.A. Obregon, R.C. Iglesias, T. Khurshaid, I. Ashraf, Smart agriculture: Utilizing machine learning and deep learning for drought stress identification in crops. Sci., 2024. 30062. https://doi.org/ 10.1038/s41598-024-74127-8.

[13]. Obahiagbon, K., and Ahonkhai, D. O., Optimized Biodiesel Production from Waste Cooking Oil Using Nickel (II) Nitrate Doped Chicken Manure as Catalyst. European Journal of Applied Sciences, 2023. 11(3), 812–824. https://doi.org/10.14738/aivp.113.14891

[14]. Masli, A, and Shamsudin, R. (2019). Sol-Gel Synthesis of Calcium Silicate Powder." AIP Conference Proceedings 2111(1). doi: 10.1063/1.5111239/888210.

[15]. Akhabue C. E., Osa-Benedict, E. O., Oyedoh, E. A., and Otoikhian, S. K., Development of a biobased bifunctional catalyst for simultaneous esterification and transesterification of neem seed oil: Modeling and optimization studies. Renewable Energy, 2020. 152, 724–735. https://doi.org/10.1016/j.renene.2020.01.103

[16]. Betiku, E., and Ishola, N. B., Optimization of sorrel oil biodiesel production by base heterogeneous catalyst from kola nut pod husk: neural intelligence genetic algorithm versus neuro-fuzzy-genetic algorithm. Environ. Prog. Sustain. Energy, 2020. 39, e13393. doi:10.1002/ep.13393

[17]. Sahin, S. and Torun, A., Comparison of engine performance and emission values of biodiesel obtained from waste pumpkin seeds with machine learning. Agriculture, 2024. 14, 227. https://doi.org/10.3390/agriculture1402022

[18]. Agadiaho, 2026

[19]. Babatunde, E. O., Karmakar, B., Olutoye, M. A., Akpan, U. G., Auta, M., and Halder, G., Parametric optimization by Taguchi L9 approach towards biodiesel production from restaurant waste oil using Fe-supported anthill catalyst. Biochemical Pharmacology, 2020. June, 104288. https://doi.org/10.1016/j.jece.2020.104288

[20]. Degfie, T. A., Mamo, T. T., and Mekonnen, Y. S., Optimized Biodiesel Production from Waste Cooking Oil (WCO) using Calcium Oxide (CaO) Nano-catalyst. Scientific Reports, 2019. 9(1), 1–8. https://doi.org/10.1038/s41598-019-55403-4

[21]. Maneerung, T., Kawi, S., Dai, Y., and Wang, C. H., Sustainable biodiesel production via transesterification of waste cooking oil by using CaO catalysts prepared from chicken manure. Energy Conversion and Management, 2016. 123, 487–497. https://doi.org/10.1016/j.enconman.2016.06.071

[22]. Alaneme, K. K., Oke S. R., Fagbayi S. B., Alabi O. O., Ojo O. M., Kareem S. A., and Folorunso D. O. Synthesis and structural analysis of calcined poultry manure for hydroxyapatite development. Next Sustainability, 2025. 5, 100079. https://doi.org/10.1016/j.nxsust.2024.100079.

[23]. Betiku, E., and Ishola, N. B., Optimization of sorrel oil biodiesel production by base heterogeneous catalyst from kola nut pod husk: neural intelligence genetic algorithm versus

neuro-fuzzy-genetic algorithm. Environ. Prog. Sustain. Energy, 2020. 39, e13393. doi:10.1002/ep.13393

[24]. Khatibi, M., Khorasheh, F., and Larimi, A., Biodiesel production via transesterification of canola oil in the presence of Na e K doped CaO derived from calcined eggshell. Renewable Energy, 2021. 163, 1626–1636. https://doi.org/10.1016/j.renene.2020.10.039

[25]. Jung, J. M., Oh, J. I., Baek, K., Lee, J., and Kwon, E. E., Biodiesel production from waste cooking oil using biochar derived from chicken manure as a porous media and catalyst. Energy Conversion and Management, 2018. 165, 628–633. https://doi.org/10.1016/j.enconman.2018.03.096

[26]. Husin, H., Riza, M., and Faisal, M., Biodiesel production using waste banana peel as renewable base catalyst. Materials Today: Proceedings, 2023. 4–7. https://doi.org/10.1016/j.matpr.2023.02.400

[27]. Mahmood, H., Iqbal, T., Haider, C., and Javaid, A., Sustainable biodiesel production from waste cooking oil utilizing waste ostrich (Struthio camelus) bones derived heterogeneous catalyst. Fuel, 2020. 277(April), 118091. https://doi.org/10.1016/j.fuel.2020.118091

[28]. Ramírez-Verduzco, L. F., Rodriguez-Rodriguezx, J. E. and Jaramillo-Jacob. Predicting cetane number, kietic viscosity, density and highe heating value of biodiesel from its fatty acid methyl ester composition. Fuel, 2012. 91, 102-111

[29]. Gouran, A., Aghel, B., and Nasirmanesh, F., Biodiesel production from waste cooking oil using wheat bran ash as a sustainable biomass. Fuel, 2021. 295(March), 120542. https://doi.org/10.1016/j.fuel.2021.120542

[30]. Ayoola, A. A., Hymore, F. K., Obande, M. A. and Udeh, I. N., Optimization of experimental conditions for biodiesel production. International Journal of Engineering and Technology, 2012. 12 (6), 130-133

[31]. Obahiagbon K., Ahonkhai D. O., Omoregie R., and Eloke P., Optimum Biodiesel Production from African Oil Bean Seed Oil Using Antelope Bones and Africa Oil Bean Seed Pod as Catalyst: RSM and ANN as Optimization Tools. European Modern Studies Journal, 2023. 7(6), 86-104. DOI: 10.59573/emsj.7(6).2023.10

[32]. Kusuma, H. S., Febryola, L. A., Rahayu, D. E., Mahfud, M., Amenaghawon, A. N., Muonanu, O. C., and Muojama, O. C., Data-driven intelligent modeling and meta-heuristic optimization of patchouli oil extraction using solvent-less microwave hydrodistillation method. Sustainable Chemistry for Climate Action, 2025. 7, 100146

[33]. Sahin, S., Comparison of machine learning algorithms for predicting diesel/biodiesel/iso-pentanol blend engine performance and emissions. Heliyon 2023. 9, e21365